analytical chemistry

pubs.acs.org/ac Article

Quantifying Antibody Binding Kinetics on Fixed Cells and Tissues *via* Fluorescence Lifetime Imaging

Prerit Mathur,[#] Anna Fomitcheva Khartchenko,[#] Stavros Stavrakis, Govind V. Kaigala,* and Andrew J. deMello*

Cite This: *Anal. Chem.* 2022, 94, 10967−10975 Read Online

ACCESS | Metrics & More | Article Recommendations | Supporting Information

ABSTRACT: We present a method for monitoring spatially localized antigen−antibody binding events on physiologically relevant substrates (cell and tissue sections) using fluorescence lifetime imaging. Specifically, we use the difference between the fluorescence decay times of fluorescently tagged antibodies in free solution and in the bound state to track the bound fraction over time and hence deduce the binding kinetics. We make use of a microfluidic probe format to minimize the mass transport effects and localize the analysis to specific regions of interest on the biological substrates. This enables measurement of binding constants (k_{on}) on surface-bound antigens and on cell blocks using model biomarkers. Finally, we directly measure p53 kinetics with differential biomarker expression in ovarian cancer tissue sections, observing that the degree of expression corresponds to the changes in k_{on}, with values of 3.27−3.50 × 10^3 M^{-1} s^{-1} for high biomarker expression and 2.27−2.79 × 10^3 M^{-1} s^{-1} for low biomarker expression.

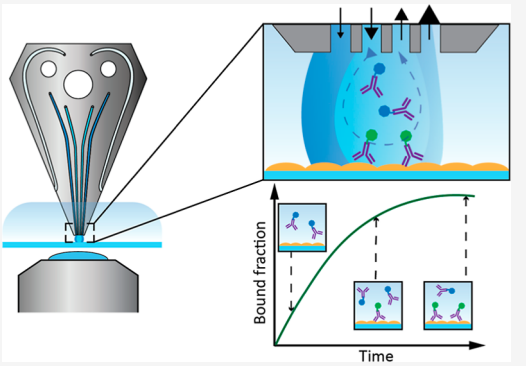

INTRODUCTION

The precise evaluation of antibody binding kinetics is essential in ensuring accurate and reproducible results in immunoassays[1] and antibody-based therapies.[2,3] Nevertheless, as a result of their production process, antibodies often suffer from batch-to-batch variations.[4] This means that many studies that use such poorly characterized antibodies cannot be reproduced.[5] The ability to generate reliable data becomes even more important for therapeutic antibodies, where the calculation of maximal dosages based on kinetic parameters must be accurate to ensure clinical efficacy.[6] While the association and dissociation parameters are constant for a specific antibody−antigen pair, their apparent values can vary depending on the concentrations of the reacting components. Such values can be further affected by the diffusion time of antibodies toward the binding site, by variations in viscosity,[7] by non-specific binding,[8] or by molecular crowding,[9] reducing the values of the association constants in cells by up to a 50%.[8] Consequently, this will affect the performance characteristics of immunoassays, such as the time required to reach equilibrium, thus resulting in poor reproducibility across multiple measurements. Accordingly, the precision in the measurement of kinetic parameters associated with antibody−antigen binding directly on the substrate of interest, such as fixed cells and tissues, is of undoubted importance.

At the current time, the most widely used approach to determine antibody kinetic parameters is surface plasmon resonance (SPR). SPR is a label-free and highly sensitive analytical technique able to resolve the kinetic parameters of a binding interaction by providing a continuous data stream.[10] That said, the exceptional sensitivity of SPR means that non-specific binding events are often difficult to distinguish from specific binding events,[11] and the measurements are extremely sensitive to local temperature variations.[12] In addition, the antibody kinetic measurements performed in SPR represent an antibody binding scenario performed in a non-native environment. Indeed, a more than one order of magnitude difference in kinetic parameters extracted from SPR systems compared to clinically derived values has been reported in multiple studies.[13,14] Although SPR is a near-field technique (with the working distance in most commercial systems being approximately 300 nm[15]), changes in the system by including two dielectrics instead of one can allow a longer range measurements and enhance the study of binding events in cells.[16] Similarly, the kinetic parameters on and within tissues can be assessed *via* quartz crystal microbalance (QCM) measurements.[17] Here, however, tissue preparation requires great care, and the tissue cannot be visualized *in situ* during the experiment, with only whole tissue kinetic analysis being

Received: March 8, 2022
Accepted: June 29, 2022
Published: July 27, 2022

https://doi.org/10.1021/acs.analchem.2c01076
Anal. Chem. 2022, 94, 10967−10975

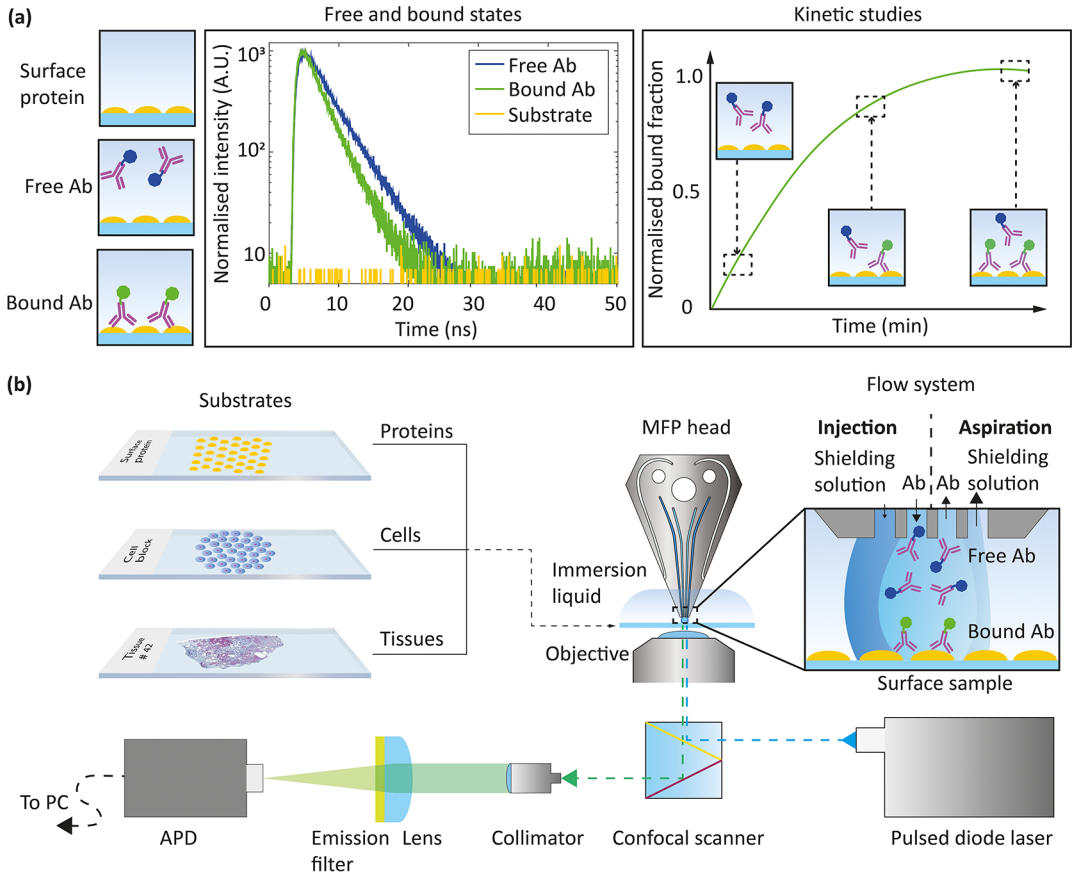

Figure 1. Working principle and workflow for kinetic analysis of antibodies. (a) Different states of the system show variable fluorescence decay time components for free and bound Ab. A change in fluorescence decay time is represented as a change in color in this figure. The surface protein is not labeled and thus has no associated lifetime. Accordingly, the proportion of the bound antibody can be tracked by monitoring the change in lifetime contribution (through the component yield or amplitude) and a kinetic curve reconstructed. (b) After choosing a substrate, an MFP is used to locally probe the regions of interest (ROIs). The setup consists of an objective, connected to a confocal scanner and an avalanche photo diode (APD). The zoomed inset shows a close-up view of the injection and aspiration apertures and highlights the confinement of an Ab solution onto a surface with proteins of interest. The size of the flow arrows indicates the relative flow rate.

possible. Thus, extracting spatially localized antibody binding information on tissues is not possible when using the aforementioned techniques.

In addition to SPR and QCM, fluorescence-based techniques offer an alternative route to probing antibody kinetics on complex surfaces. However, since fluorescence intensity-based measurements cannot easily distinguish between free and bound molecules, such approaches require constant removal of excess of fluorescent species during the experiment, which limits their applicability in real-world scenarios. For example, Ostromohov *et al.* developed a microfluidic device that inserts buffer plugs for washing and gives some seconds for obtaining the image of the bound fraction of the antibodies.[18] Kashyap *et al.* used a microfluidic device to deliver a primary antibody on different tissue regions, with the signal being revealed *via* a secondary antibody.[19] Additionally, Bondza *et al.* used cells cultured on a rotating plate while alternating between an incubation and imaging area to avoid background issues.[20] In all these cases, the need to remove the excess fluorescence for real-time observation resulted in these creative strategies, which, while giving semiquantitative values to the kinetic constant, present a larger possibility of error accumulation due to the complexity of the measured system. This shortcoming can in principle be overcome through the adoption of fluorescence lifetime imaging (FLIM), where the measured fluorescence decay time components are largely independent of fluorophore concentrations.[21] FLIM is able to probe variations in the molecular environment, being used to detect changes in pH[22] and viscosity,[23] molecular binding,[24] and even to identify malignant tissues.[25] It is useful to note that fluorescence lifetime depends only on the local properties of a sample, and thus, accounting for these properties is easier as compared to environmental factors such as temperature. The temporal analysis of such molecular environmental changes has successfully been used to calculate the reaction kinetics,[26] crystallization rates of pharmaceutical compounds,[27] and protein aggregation in animal models.[28] Additionally, it is interesting to note that FLIM has been used to characterize the binding of small molecules to kinases using the differences in the fluorescence decay time between bound and unbound states.[29] Accordingly, FLIM offers a potentially useful way to analyze the binding kinetics of antigen and antibody pairs.

Herein, we present a new methodology combining open-space microfluidics with FLIM for spatially localized quantitative measurements of antibody−antigen binding on various substrates, including cells and clinical tissue samples. Importantly, we measure the binding constant of the binding reaction with the assumption that the dissociation constant is negligible in comparison to association and thus has negligible

https://doi.org/10.1021/acs.analchem.2c01076
Anal. Chem. 2022, 94, 10967−10975

effects for the duration of our measurement. To the best of our knowledge, this is the first study that reports the measurement of binding events on clinical tissue samples and maps their location. As a proof of concept, we monitor the real-time binding kinetics of immunoglobulin (IgG) to fluorescently labeled anti-IgG antigens immobilized on the surface of cells or tissues (Figure 1a). We use a microfluidic probe (MFP) (Figure 1b), a device able to localize chemicals on a surface through confinement of microflows,[19] to generate an advective flow and thus allow operation in a reaction-limited setting. Using the localization capabilities of the MFP, we examine specific ROIs within cell blocks and cancer tissue sections. Significantly, we observe a variation in kinetics over the tissue section, a product of differential expression of biomarkers in these tissues.

EXPERIMENTAL SECTION

Additional details about the materials and methods can be found in the Supporting Information (Supporting Note 1).

FLIM Platform. Fluorescence lifetime measurements were performed using the custom system shown in Figure S1. A picosecond pulsed diode laser (PDL-800 D) (PicoQuant, Germany) was used with an excitation wavelength of 488 ± 5 nm at a repetition rate of 20 MHz (peak power ≈ 2.5 mW). The output was coupled through an optical fiber to a C2si confocal scanner controlling a Nikon Eclipse Ti inverted microscope (Nikon, Switzerland). Emitted photons were routed through an optical fiber to a collimator (F950FC-A, Thorlabs, Germany), after which it was focused with a doublet lens (AC254-050-A, Thorlabs, Germany), passed through a 496 nm wavelength long-pass filter (AHF, Germany) and detected by an avalanche photodiode-based single-photon counting module (SPCM-AQRH, Excelitas Technologies, USA). The Nikon scanner and laser detection setups were controlled by separate computers, with both communicating to each other over a home network in a master-slave configuration. The software NIS Elements C (Nikon, Switzerland) was used to control the scanner, and SymPhoTime 64 (PicoQuant, Germany) was used to collect the lifetime data. Time decay parameters were also calculated with the SymPhoTime 64 software.

Microfluidic Probe Setup. An MFP was fabricated as described elsewhere.[30] Briefly, channels were etched on a silicon wafer, which was then anodically bonded to a glass slide. The MFP heads were then diced and cleaned. Prior to an experiment, the MFP was sonicated in a 1:1 mixture of ethanol and isopropanol for 5 min. Then, the head was attached to a holder using circular connectors (Dolomite Microfluidics, UK), which also provides guide connections for Teflon fluid tubing (1/32″). The flow was controlled by four Nemesys syringe pumps (Cetoni GmbH, Germany) (Figure S1). The MFP functions by delivering the fluid through an injection channel and aspirating simultaneously with at least three times the flow rate of the injection, creating a flow confinement on the surface of interest. The sample must be submerged in the meantime. In the current work, we used a hierarchical hydrodynamic flow confinement,[31] that is, the use of a shielding liquid around the flow confinement to reduce the diffusion of analyte outside the confinement.

Fluorescence Lifetime Measurements on Antigen-Labeled Surfaces On Bench. Rabbit IgG (50 μL, 50 μg/mL, Sigma-Aldrich, Switzerland) was deposited for 1 h on the surface of a glass slide. The surface was then washed with 100 μL of phosphate-buffered saline (PBS) three times to remove non-adherent antibodies. Bovine serum albumin (BSA, 1%) in PBS buffer was used to block the open sites on the surface and left to incubate in the dark for 30 min. Again, the surface was washed with 100 μL of PBS three times to remove the unspecifically bound moieties. We used goat anti-rabbit Alexa 488 labeled IgG H&L (Abcam, Germany) as a detection antibody.

A similar procedure was performed for the p53 biomarker. Recombinant human p53 protein, CF (50 μL, 50 μg/mL, Bio-Techne AG, Switzerland), was deposited for 1 h on the surface of a glass slide. The surface was then washed with 100 μL of PBS three times to remove non-adherent antibodies. BSA (1%) in PBS buffer was used to block the open sites on the surface and left to incubate in the dark for 1 h. Again, the surface was washed with 100 μL of PBS three times to remove the unspecifically bound moieties. We used recombinant anti-p53 antibody [E26] conjugated with Alexa 488 (20 μg/mL, Abcam, Germany) (termed as anti-p53 A488) as a detection antibody.

Fluorescence Lifetime Measurements on Antigen-Labeled Surfaces Using Flow. A glass slide was prepared as described above. Next, an MFP was used to drive the flow of anti-rabbit Alexa 488 IgG in the inner confinement on the rabbit-IgG surface. PBS was used as an immersion liquid and in the shielding liquid. The flow rates were set to 0.2 μL/min for outer injection, 2 μL/min for inner injection, 2 μL/min for inner aspiration, and 4.6 μL/min for outer aspiration. The time was set to $t = 0$ when the flow was turned on. The fluorescence decay times were measured at a fixed region in the confinement at several time points. All measurements were performed at the same spot to avoid issues related to uneven surface coverage.

Cell Blocks and Tissues. Cell blocks MDA-MB-231, SKBR3 (AMS Biotechnology, UK), and tissues provided by the University Hospital Zurich were used as substrates. The retrospective use of tumor tissues of the patients is in accordance with the Swiss Human Research Law "Humanforschungsgesetz (HFG)". The study was approved by the cantonal commission of ethics of Zurich (BASEC-no. 2019-01477). Prior to use, the cell blocks and tissues were dewaxed. Briefly, the formalin-fixed, paraffin-embedded tissue section was incubated in xylene twice for 5 min each to remove the wax. Afterward, to remove xylene and rehydrate the tissue, the section was washed in a 1:1 mixture of ethanol and xylene (3 min), twice in pure ethanol (3 min each), twice in 95% ethanol (3 min each), and in tap water (3 min). All washing steps were performed by shaking the sample. Finally, the section underwent antigen retrieval in an antigen retrieval solution (Dako, Denmark) at 90 °C for 20 min and was allowed to cool for 40 min. The sections were then used immediately.

Fluorescence Lifetime Measurements for Cell Blocks and Tissues under Flow. A cell block or a tissue section was first prepared as detailed above. Then, 1% BSA in PBS buffer was used to block open sites on the surface and left to incubate in the dark for 1 h. Further, an MFP was used to drive the flow of the antigen in the inner confinement on the cell or tissue surface. PBS was used as the immersion liquid and in the shielding liquid. The flow rates were set to 0.2 μL/min for outer injection, 2 μL/min for inner injection, 2 μL/min for inner aspiration, and 4.6 μL/min for outer aspiration. The time was set at $t = 0$ when the Ab flow was turned on. The fluorescence decay times were measured at a fixed region in the confinement at several time points. All measurements over

https://doi.org/10.1021/acs.analchem.2c01076
Anal. Chem. 2022, 94, 10967−10975

time were performed at the same spot to avoid issues due to uneven surface coverage. The antigen used was either recombinant anti-p53 antibody [E26] conjugated with Alexa 488 (20 μg/mL, Abcam, Germany) or rabbit monoclonal [EPR19547-12] antibody to ErbB2 conjugated with Alexa 488 (20 μg/mL, Abcam, Germany) depending on the substrate.

RESULTS AND DISCUSSION

Working Principle: Measurement of Bound Antibody Fraction on a Surface. Fluorescently labeled antibodies present different decay time characteristics in free solution than when bound to a surface[29] (Figure 1a), while the unlabeled antigens, such as the ones present on the surface, will exhibit no fluorescence lifetime. During the reaction, both free and bound species will be present, and thus, the measured decay, $F(t)$, can be modeled by a biexponential decay function (eq 1), where τ_1 and τ_2 represent the average fluorescence lifetimes of the free and bound species, respectively, with the pre-exponential factors α_1 and α_2 reporting their relative proportions.[32]

$$F(t) = I_0\left[\alpha_1 \exp\left(-\frac{t}{\tau_1}\right) + \alpha_2 \exp\left(-\frac{t}{\tau_2}\right)\right] \quad (1)$$

Importantly, eq 1 enables the relative proportion of bound and unbound species to be extracted at a given time point in an experiment. Initially, we used FLIM to measure antigen–antibody binding kinetics of the rabbit–anti-rabbit IgG pair on plain glass slides (Figure 2a). Specifically, we probed the binding of anti-rabbit IgG labeled with Alexa 488 (in solution) to unlabeled rabbit IgG coated on a glass surface. The free and bound A488-labeled IgG presented lifetimes of 3.79 ± 0.03 and 2.79 ± 0.09 ns, respectively, allowing us to simply discriminate between the two states. It is interesting to note that both these lifetimes were lower than the free state lifetime of Alexa 488, which was 4.08 ± 0.02 ns (in agreement with values reported in the literature of 4.1 ns[33]). Such fluorophore quenching due to the presence of organic dyes bound to proteins and antibodies has been previously reported in the literature.[34−36] We then proceeded to evaluate the evolution of the ratio between bound and free states as a function of time, with time-integrated fluorescence measurements (fluorescence intensity measurements) used as a control. As can be seen in Figure 2b, time-integrated and time-resolved measurements showed excellent agreement over the time course of the experiment.

Measurement of Binding Kinetics on Surface-Bound Antigens and on Fixed Cells. To provide an accurate measurement of the kinetics of a system, any analytical method must consider the effects of mass transport in the reaction. To determine the relative effect of the reaction rate to the transport rate, we use the Damköhler number (Da)

$$Da = \frac{k_{on} b_m \delta}{D} \quad (2)$$

where k_{on} represents the association constant, b_m the number of binding sites on a surface, δ the size of the depletion layer, and D the diffusion coefficient of the molecule. When $Da \gg 1$, the reaction will be transport limited and thus not suitable for reaction kinetics measurements. This is the case for the scenario depicted in Figure 2a, where the depletion layer (the region where the analyte is consumed) increases with time, limiting the reaction (we term these experimental settings "on bench"). The size of the depletion layer (δ) grows with time (t) at the rate given by[37]

$$\delta = \sqrt{2Dt} \quad (3)$$

For an antibody diffusivity of $D = 1 \times 10^{-11}$ m^2/s, analysis of eq 3 indicates that the depletion layer increases from 109 μm at 10 min to 268 μm after 1 h. This in turn causes a progressive increase in Da and thus a reduction in reaction rate. Accordingly, to measure the kinetic parameters, the dependency of transport must be removed, which can be achieved by generating advection. To realize a low Da, we use the MFP to deliver a bespoke flow rate on the ROI. Importantly, the presence of the flow maintains a constant depletion layer, unlike the on-bench experiment, where it constantly increases. In this case, using an injection flow rate of 2 μL/min, Da is

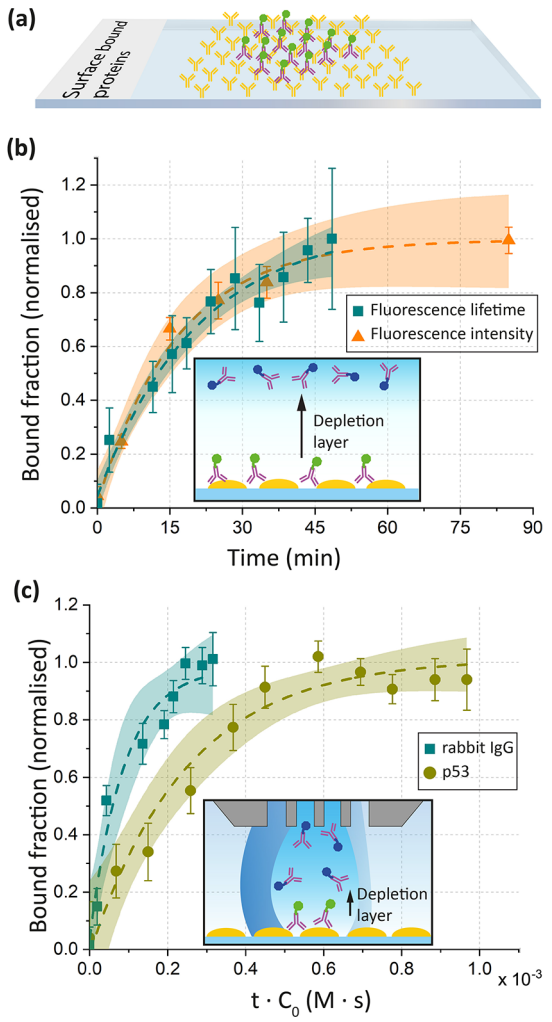

Figure 2. Kinetic analysis of antibody binding on surface-bound proteins. (a) Schematic of the measurement principle when evaluating bound Ab fractions on a glass substrate. (b) Variation of fluorescence intensity and fluorescence lifetime as a function of time for the binding of rabbit IgG–anti-rabbit A488 pair on a plain glass substrate. (c) Kinetic curves for binding of rabbit–anti-rabbit A488 and p53–anti-p53 A488 pairs on a plain glass slide, with MFP-generated flows. Insets show the relative size of the depletion layer in both scenarios. Error bars at each point represent the standard error associated with a biexponential fit, and shaded regions represent the 95% confidence interval of the kinetic curve fit.

https://doi.org/10.1021/acs.analchem.2c01076
Anal. Chem. 2022, 94, 10967−10975

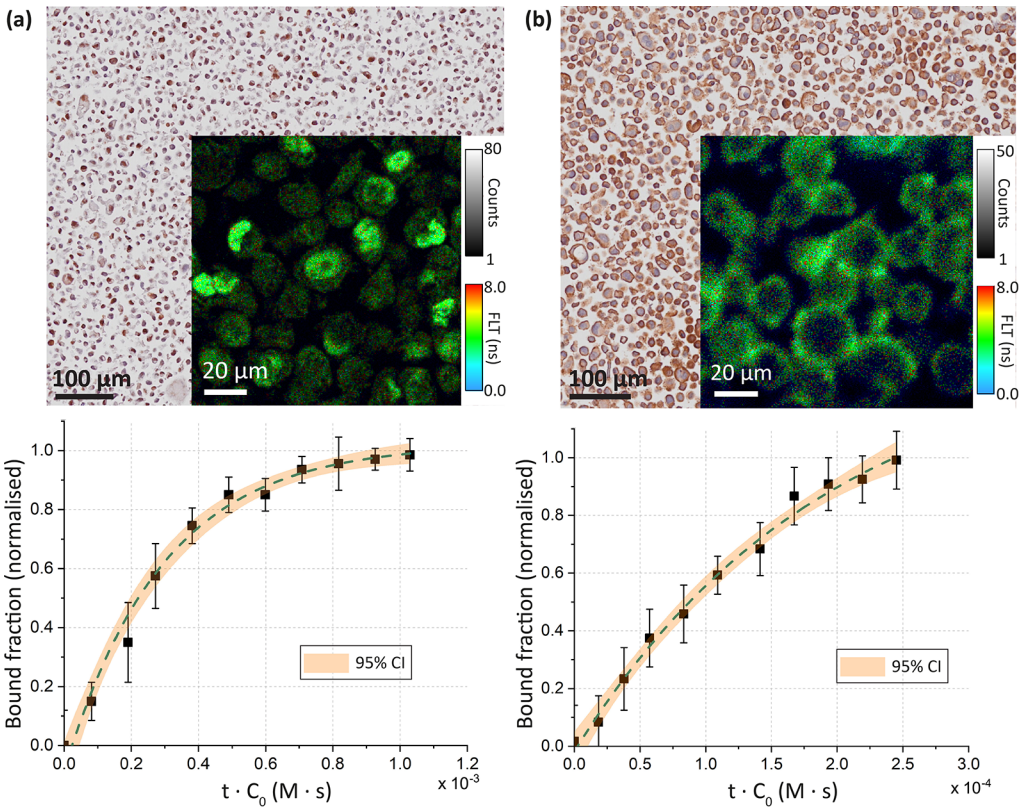

Figure 3. Kinetic analysis of antibody binding on cell blocks. (a) MDA-MB-231 expressing p53 (top panel). The inset shows an associated fluorescence lifetime map. The bottom panel shows the kinetic curve for binding of anti-p53-A488 to the cell block. (b) Top panel shows SKBR3 cells expressing HER2. The inset shows an associated fluorescence lifetime map. The bottom panel represents the kinetic curve of anti-HER2-A488 binding to SKBR3. In both cases, the dashed line represents the best fit for k_{on} calculation. The error bars at each point represent standard error of a biexponential fit, and the shaded region represents the 95% confidence interval of the kinetic curve fit.

approximately 0.12, corresponding to a depletion layer of 3.97 μm, calculated by eq 4

$$\delta = \left(\frac{DLWH^2}{3Q}\right)^{1/3} \tag{4}$$

Here, W and L correspond to the length and width of the flow confinement, respectively, H is the distance from the probe to the surface, and Q is the flow rate.[38] We use $k_{on} = 1 \times 10^4$ M^{-1} s^{-1}, $L = W = 500$ μm, $H = 50$ μm, and $b_m = 2.98 \times 10^{-8}$ mol m^{-2} for our approximate calculations.[38] Higher flow rates will result in even smaller depletion layers. However, for a kinetic experiment, where the time range is on the order of tens of minutes, this would result in excessively high analyte consumption.

When calculating the association constant k_{on}, we assume a pseudo-first-order reaction as the free antibody is always present in excess (and replenished by the flow), and thus, its concentration can be considered to be constant over time. Thus, for the antibody−antigen complex, P, and the antigen, Ag, we can write

$$\frac{\partial[\mathrm{P}]}{\partial t} = k'_{on}[\mathrm{Ag}] \tag{5}$$

where k'_{on} is the apparent binding rate. The term k'_{on} includes the initial concentration of the antibody, c, *via* the relation $k'_{on} = k_{on}c$, where c is assumed to be constant throughout the experiment. The concentration, c, used in each experiment is found in the Experimental Section. For the previously described rabbit−anti-rabbit A488 system, we obtained a k_{on} of $1.14 \pm 0.41 \times 10^4$ M^{-1} s^{-1} (Figure 2c), which is in good agreement with the literature.[39]

While kinetic measurements on a surface are useful to obtain the kinetic parameters, the binding between an antibody and its antigen is often associated with cells or tissues due to the biological complexity which these present.[20] Accordingly, we assessed the kinetics of biomarker binding on cell blocks. Such measurements are presented in Figure 3. We tested MDA-MB-231, a breast-cancer-derived cell line that overexpresses p53, a common mutation in cancer.[40] The analysis of the fluorescence lifetime of the antibody in its free state and cell-bound state yields lifetimes of 3.83 ± 0.06 and 3.44 ± 0.09 ns, respectively, sufficient to differentiate them and allow FLIM-based kinetic measurements. Importantly, the cell block does not present autofluorescence for the excitation and emission ranges used. Using an MFP to drive a flow of anti-p53 labeled with A488 onto the cell block, we performed a kinetic analysis, obtaining a k_{on} of $3.46 \pm 0.31 \times 10^3$ M^{-1} s^{-1} (Figure 3a). For comparison, we also performed the k'_{on} analysis on p53-coated glass slides. In this case, the average lifetime of the bound-state antibody was 2.76 ± 0.08 ns and $k_{on} = 3.29 \pm 0.32 \times 10^3$ M^{-1} s^{-1} (Figure 2c). Such variations of the rate constants are likely due to the time required for the antibodies to diffuse to their binding sites.

To demonstrate the reliability of our approach for analyzing multiple biomarkers, we measured the kinetic constant using an SKBR3 cell block, a breast adenocarcinoma-derived cell line overexpressing human epidermal growth factor receptor 2

https://doi.org/10.1021/acs.analchem.2c01076
Anal. Chem. 2022, 94, 10967−10975

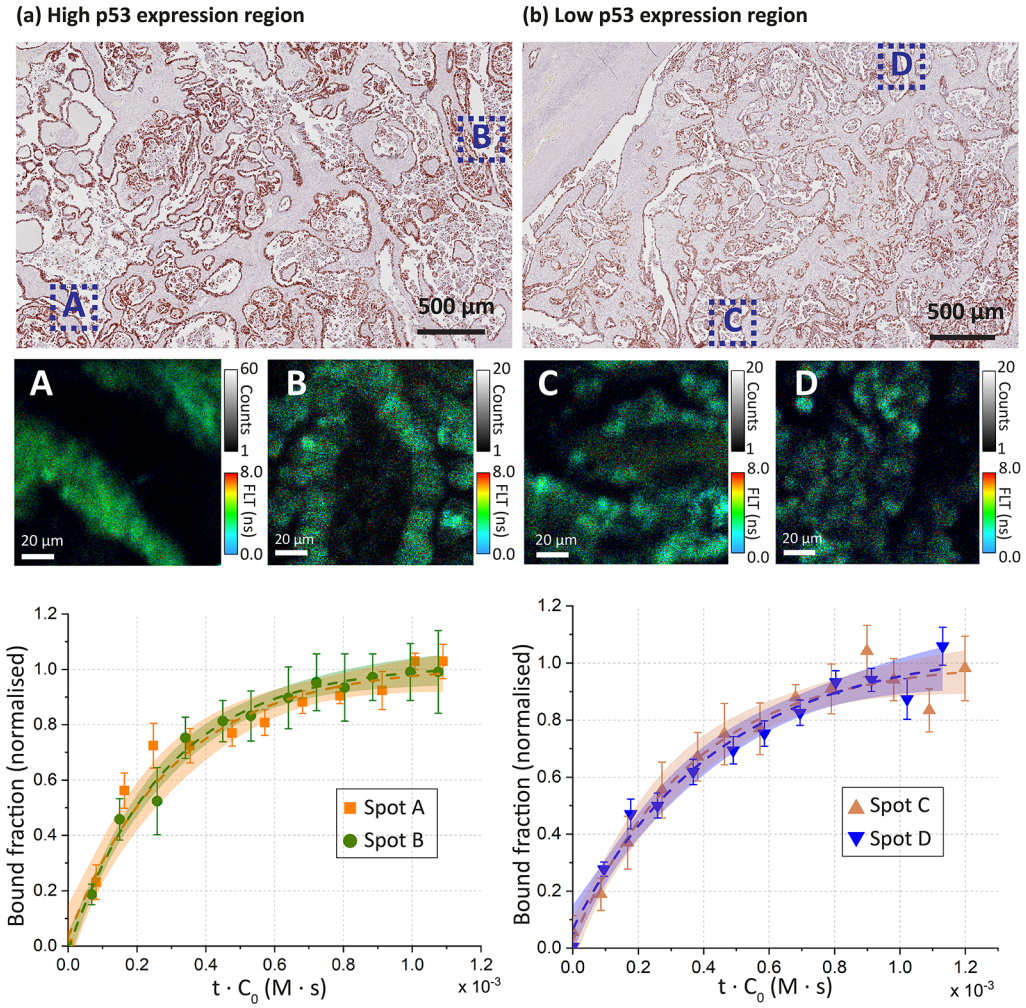

Figure 4. Binding kinetics on a human ovarian cancer tissue section overexpressing p53. (a) Region of high expression and (b) region of low expression determined by IHC (top panel). Regions A, B, C, and D are marked on the tissue section and correspond to the selected regions of analysis using FLIM. The bottom panels show the binding kinetics of the corresponding regions. The error bars at each point represent the standard error of a biexponential fit, and the shaded region represents the 95% confidence interval of kinetic curve analysis.

(HER2), a membrane protein used for breast cancer subtyping.[41] In this case, the free and bound-state lifetimes of anti-HER2 A488 were 3.76 ± 0.01 and 3.36 ± 0.11 ns, respectively, and a k_{on} of 5.39 ± 1.49 × 10^3 M^{-1} s^{-1} was extracted (Figure 3b). Additionally, we performed a comparison between the kinetics observed using conventional immunofluorescence test and our approach with FLIM to evaluate the viability of FLIM to determine the k'_{on} values. We performed this comparison on surfaces (Figure 2b) and cell blocks (Supporting Note 3) for completeness. The obtained kinetic behavior by immunofluorescence and FLIM on both surfaces and cell blocks was very similar. This confirmed that our assay was as good as the gold standard immunofluorescence, with the additional advantages of spatial localization, flow-enhanced mass transport, simplified assay procedure for kinetic measurements, higher time resolution, and consequently better confidence intervals for curve fits. Additionally, we performed a negative control to ensure that measurements do not have a systematic bias due to non-specific interactions. Here, we used the MFP to flow anti-HER2 conjugated with Alexa 488 onto a glass slide passivated with BSA. Significantly, we observed that the fluorescence lifetime does not change over time, confirming that there are no unspecific bound species interactions (Supporting Note 4).

Evaluation of p53 Expression on Cancer Tissues Using Kinetic Analysis. To demonstrate the utility of our method in clinically relevant samples, we performed a kinetic analysis on a patient-derived ovarian cancer tissue, a cancer type that often overexpresses p53.[42] Due to autofluorescence at 488 nm (due to collagen, elastin, and other endogenous molecules,[43] shown in Figure S2), we used a *TrueBlack* quencher to dramatically reduce the autofluorescence associated with the tissue (Figure S3). Using a quencher was necessary to obtain signals from the binding events, which might not present strong intensities due to a limited antigen density on the tissue. This was not the case for cell blocks, which exhibit no autofluorescence, as the autofluorescence seems to be derived mostly from proteins in the extracellular matrix. The bound-state lifetime for anti-p53 A488 on quenched tissues was found to be 2.54 ± 0.18 ns. This value is lower than the bound-state anti-p53 A488 lifetime in cell blocks due to the presence of the quencher. To test the efficacy of our method in tissues, we chose two regions on the basis of a p53 immunohistochemical (IHC) map—one with high expression of p53 and the other with low expression (Figures 4

https://doi.org/10.1021/acs.analchem.2c01076
Anal. Chem. 2022, 94, 10967−10975

and S4), since tumors typically exhibit heterogeneity in protein expression.[44] Two spots within each region were probed and used to extract the kinetic constant. Spot A and B show higher expression levels than spots C and D on the IHC map. The k_{on} values obtained were $3.50 \pm 0.37 \times 10^3$ and $3.27 \pm 0.59 \times 10^3$ M^{-1} s^{-1} for the high-expression spots A and B, respectively, and $2.79 \pm 0.47 \times 10^3$ and $2.27 \pm 0.41 \times 10^3$ M^{-1} s^{-1} for the low-expression spots C and D, respectively (Figure 4). These values indicate a tendency for faster kinetics on regions associated with high protein expression, since under conditions of antibody excess, this value will depend on antigen concentration on the surface. While the high heterogeneity of p53 even in localized regions produces a certain error in the measurement, the obtained value gives an excellent indication of the biomarker surface density. Accordingly, our method can be used as a tool for protein expression quantification using kinetics.

CONCLUSIONS

In this work, we have demonstrated that the binding of an antigen and an antibody can be evaluated using FLIM and proposed a strategy to analyze antigen−antibody binding kinetics on localized regions of cell blocks and tissues. We observe that in the case of labeled moieties, which exhibit fluorescence, it is possible to follow the binding reactions by observing changes in the component decay times and extracting the proportion of bound-state antibody as a function of time. Our method only requires the modification of one of the moieties, contrary to FLIM-FRET (Förster resonance energy transfer) methods commonly used to follow protein binding, which require modifying both donor and acceptor molecules.

The bound-state fluorescence lifetimes of antigens are different from the associated free-state lifetimes for two main reasons. First, binding causes a change in the local microenvironment and a reduction in the degree of freedom of a molecule, both of which will have a significant effect on the fluorescence decay time components. Second, the refractive index of the surface, cells, and tissues will also be different from the bulk solution, which will also cause a variation in the fluorescence lifetime.[45] Specifically, for the case of tissue sections, the presence of an autofluorescence quencher bound to the tissue will also reduce the lifetime of the tissue-bound antigen.[46]

To reduce the dependency on mass transport, our system leverages microflows to deliver antibodies to the surface. Since the effects of mass transport are not always observable experimentally, estimating the expected mass transport before an experiment is critical in obtaining accurate kinetic values.[47] The use of the MFP to reduce mass transport offers the additional and significant advantage of localizing the signal in a ROI. The current work focuses on measuring tissue level kinetics. Thus, we chose our ROI to cover 20−30 cells and obtained an average binding constant over this region. It should be possible to perform similar analysis on smaller ROIs (approximately 10 μm in size, down to a single-cell level). The requirement would be to have a higher magnification and higher numerical aperture objective to collect enough photons for FLIM analysis.

A better understanding of binding kinetics is invaluable in choosing the best antibodies when performing immunoassays and immunohistochemistry. In addition, by leveraging the localization capabilities of the MFP, we could successfully evaluate the binding of several antibodies of interest in a parallel fashion and directly on tissues. Such additional characterization is likely to be critical in obtaining standardized and reproducible immunoassays.[48] Moreover, an understanding of the kinetics of tissue binding is likely to be critical in predicting the effects of drugs. Indeed, k_{on} values have previously been shown to determine the binding and rebinding capacity of therapeutic drugs.[49] In addition, we show that our method can be leveraged for kinetic investigations in malignant or disease-related tissues, which is of high clinical importance.[50] Such binding is to a great extent affected by the biomarker density, having been used for quantification of antigen expression on tissues.[19] Here, we show that changes in k_{on} based on the expression of surface biomarkers are indeed correlated with the observed protein expression. While local analysis can provide a certain degree of quantification, the time to make such measurements can be unacceptably long. To avoid such a shortcoming, we envision a microfluidic platform that would cover the whole tissue section while performing high-resolution FLIM in real time. This would permit the analysis of heterogeneity in expression based on the kinetics of binding in the whole tissue in a single experiment. We expect that the use of kinetic analyses will offer the possibility of quantifying protein expression in different patients since we observe such differences even within the same tumor. Accordingly, we believe that our method offers an alternative way of analyzing antigen−antibody binding kinetics, offering the additional advantage of locally analyzing the binding kinetics on cells and tissues.

ASSOCIATED CONTENT

Supporting Information

The Supporting Information is available free of charge at https://pubs.acs.org/doi/10.1021/acs.analchem.2c01076.

Materials and methods, biexponential fluorescence lifetime fits, comparison of fluorescence intensity and lifetime on cells, negative control for unspecific binding, comparison between flow and on-bench scenarios, and effect of photobleaching (PDF)

AUTHOR INFORMATION

Corresponding Authors

Govind V. Kaigala − *IBM Research Europe—Zurich, CH-8803 Rüschlikon, Switzerland; School of Biomedical Engineering, University of British Columbia, Vancouver BC V6T 1Z3, Canada;* orcid.org/0000-0003-1145-7287; Email: govind.kaigala@ubc.ca

Andrew J. deMello − *Institute for Chemical and Bioengineering, Department of Chemistry & Applied Biosciences, Eidgenössische Technische Hochschule (ETH Zürich), 8093 Zürich, Switzerland;* orcid.org/0000-0003-1943-1356; Email: andrew.demello@chem.ethz.ch

Authors

Prerit Mathur − *Institute for Chemical and Bioengineering, Department of Chemistry & Applied Biosciences, Eidgenössische Technische Hochschule (ETH Zürich), 8093 Zürich, Switzerland; IBM Research Europe—Zurich, CH-8803 Rüschlikon, Switzerland*

Anna Fomitcheva Khartchenko − *Institute for Chemical and Bioengineering, Department of Chemistry & Applied Biosciences, Eidgenössische Technische Hochschule (ETH*

Zürich), 8093 Zürich, Switzerland; IBM Research Europe—Zurich, CH-8803 Rüschlikon, Switzerland

Stavros Stavrakis − *Institute for Chemical and Bioengineering, Department of Chemistry & Applied Biosciences, Eidgenössische Technische Hochschule (ETH Zürich), 8093 Zürich, Switzerland;* orcid.org/0000-0002-0888-5953

Complete contact information is available at: https://pubs.acs.org/10.1021/acs.analchem.2c01076

Author Contributions

#P.M. and A.F.K. contributed equally. P.M., A.F.K., G.V.K., and A.dM. conceived the study. P.M. and S.S. designed the experimental setup. P.M. and A.F.K. designed the experiments and analyzed the data. P.M. performed the experiments. All authors contributed to writing the manuscript.

Notes

The authors declare no competing financial interest.

■ ACKNOWLEDGMENTS

We would like to thank I. Pereiro, A. Kashyap, A. Jain, J. Probst, and P. Schraml for helpful discussions. P. Schraml, S. Dettwiler, and F. Prutek (Tissue Biobank, University Hospital Zurich) are acknowledged for providing tissue samples. We also thank E. Delamarche and H. Riel for constant support. We acknowledge support from the staff at Binning and Rohrer Nanotechnology Center (BRNC) on the IBM Research Europe campus for help in fabricating the microfluidic devices. We thank Anel Zulji for support in device fabrication. Research reported in this publication was funded, in part, by the European Research Council (ERC) PoC grant (project no. 842790, CellProbe) and the Swiss National Science Foundation (grant number: 205321/176011). We additionally acknowledge partial support from ETH Zürich.

■ REFERENCES

(1) Place, J. F.; Sutherland, R. M.; Riley, A.; Mangan, C. Immunoassay Kinetics at Continuous Surfaces. In *Biosensors with Fiberoptics*; Wise, D. L., Wingard, L. B., Eds.; Humana Press: Totowa, NJ, 1991; pp 253−291.
(2) Langmuir, V. K.; Mendonca, H. L.; Woo, D. V. *Cancer Res.* **1992**, *52*, 4728−4734.
(3) Borrebaeck, C. A. K.; Malmborg, A. C.; Furebring, C.; Michaelsson, A.; Ward, S.; Danielsson, L.; Ohlin, M. *Nat. Biotechnol.* **1992**, *10*, 697−698.
(4) Bradbury, A.; Plückthun, A. *Nature* **2015**, *518*, 27−29.
(5) Begley, C. G.; Ellis, L. M. *Nature* **2012**, *483*, 531−533.
(6) Wang, M.; Kussrow, A. K.; Ocana, M. F.; Chabot, J. R.; Lepsy, C. S.; Bornhop, D. J.; O'Hara, D. M. *Br. J. Pharmacol.* **2017**, *174*, 70−81.
(7) Wang, Y.; Li, C.; Pielak, G. J. *J. Am. Chem. Soc.* **2010**, *132*, 9392−9397.
(8) Phillip, Y.; Kiss, V.; Schreiber, G. *Proc. Natl. Acad. Sci. U.S.A.* **2012**, *109*, 1461−1466.
(9) Verkman, A. S. *Trends Biochem. Sci.* **2002**, *27*, 27−33.
(10) Hearty, S.; Leonard, P.; Ma, H.; O'Kennedy, R. Measuring Antibody-Antigen Binding Kinetics Using Surface Plasmon Resonance. In *Methods in Molecular Biology*; Humana Press Inc., 2018; Vol. *1827*, pp 421−455.
(11) Helmerhorst, E.; Chandler, D. J.; Nussio, M.; Mamotte, C. D. Real-Time and Label-Free Bio-Sensing of Molecular Interactions by Surface Plasmon Resonance: A Laboratory Medicine Perspective. *Clinical Biochemist Reviews*; The Australian Association of Clinical Biochemists, 2012; pp 161−173.
(12) Scarano, S.; Mascini, M.; Turner, A. P. F.; Minunni, M. *Biosens. Bioelectron.* **2010**, *25*, 957−966.
(13) Martin, S. W.; Magnusson, M. O.; Matthews, I. T.; Burgess, G.; Niezychowski, W. *Gastroenterology* **2009**, *136*, A-641.
(14) Brodfuehrer, J.; Rankin, A.; Edmonds, J.; Keegan, S.; Andreyeva, T.; Lawrence-Henderson, R.; Ozer, J.; Gao, H.; Bloom, L.; Boisvert, A.; Lam, K.; Lee, J.; LaBranche, T.; Syed, J.; Miao, W.; Singh, P. *Pharm. Res.* **2014**, *31*, 635−648.
(15) Olaru, A.; Bala, C.; Jaffrezic-Renault, N.; Aboul-Enein, H. Y. *Crit. Rev. Anal. Chem.* **2015**, *45*, 97−105.
(16) Yanase, Y.; Hiragun, T.; Ishii, K.; Kawaguchi, T.; Yanase, T.; Kawai, M.; Sakamoto, K.; Hide, M. *Sensors* **2014**, *14*, 4948−4959.
(17) Clausen, T. M.; Pereira, M. A.; Oo, H. Z.; Resende, M.; Gustavson, T.; Mao, Y.; Sugiura, N.; Liew, J.; Fazli, L.; Theander, T. G.; Daugaard, M.; Salanti, A. *Sens. Bio-Sens. Res.* **2016**, *9*, 23−30.
(18) Ostromohov, N.; Bercovici, M.; Kaigala, G. V. *Lab Chip* **2016**, *16*, 3015−3023.
(19) Kashyap, A.; Fomitcheva Khartchenko, A.; Pati, P.; Gabrani, M.; Schraml, P.; Kaigala, G. V. *Nat. Biomed. Eng.* **2019**, *3*, 478−490.
(20) Bondza, S.; Foy, E.; Brooks, J.; Andersson, K.; Robinson, J.; Richalet, P.; Buijs, J. *Front. Immunol.* **2017**, *8*, 455.
(21) van Munster, E. B.; Gadella, T. W. J. Fluorescence Lifetime Imaging Microscopy (FLIM). *Advances in Biochemical Engineering/Biotechnology*; Springer: Berlin, Heidelberg, March 27, 2005; pp 143−175.
(22) Ryder, A. G.; Power, S.; Glynn, T. J.; Morrison, J. J. Time-Domain Measurement of Fluorescence Lifetime Variation with PH. In *BiOS 2001 The International Symposium on Biomedical Optics*; Bearman, G. H., Bornhop, D. J., Levenson, R. M., Eds.; SPIE, 2001; Vol. *4259*, pp 102−109.
(23) Haidekker, M. A.; Theodorakis, E. A. *Org. Biomol. Chem.* **2007**, *5*, 1669−1678.
(24) Lebakken, C. S.; Kang, H.; Vogel, K. W. *J. Biomol. Screening* **2007**, *12*, 828−841.
(25) Tadrous, P. J.; Siegel, J.; French, P. M. W.; Shousha, S.; Lalani, E.; Stamp, G. W. H. *J. Pathol.* **2003**, *199*, 309−317.
(26) Matthews, S. M.; Elder, A. D.; Yunus, K.; Kaminski, C. F.; Brennan, C. M.; Fisher, A. C. *Anal. Chem.* **2007**, *79*, 4101−4109.
(27) Rautaniemi, K.; Vuorimaa-Laukkanen, E.; Strachan, C. J.; Laaksonen, T. *Mol. Pharm.* **2018**, *15*, 1964−1971.
(28) Laine, R. F.; Sinnige, T.; Ma, K. Y.; Haack, A. J.; Poudel, C.; Gaida, P.; Curry, N.; Perni, M.; Nollen, E. A. A.; Dobson, C. M.; Vendruscolo, M.; Kaminski Schierle, G. S.; Kaminski, C. F. *ACS Chem. Biol.* **2019**, *14*, 1628−1636.
(29) Lebakken, C. S.; Kang, H.; Vogel, K. W. *J. Biomol. Screening* **2007**, *12*, 828−841.
(30) Kaigala, G. V.; Lovchik, R. D.; Drechsler, U.; Delamarche, E. *Langmuir* **2011**, *27*, 5686−5693.
(31) Autebert, J.; Kashyap, A.; Lovchik, R. D.; Delamarche, E.; Kaigala, G. V. *Langmuir* **2014**, *30*, 3640−3645.
(32) Lakowicz, J. R. *Principles of Fluorescence Spectroscopy*; Springer, 2006.
(33) Chapter 20: PH Indicators. In *The Molecular Probes Handbook: A Guide to Fluorescent Probes and Labeling Technologies*; ThermoFisher Scientific, 2010.
(34) Alcala, J. R.; Gratton, E.; Prendergast, F. G. *Biophys. J.* **1987**, *51*, 597−604.
(35) Borst, J. W.; Willemse, M.; Slijkhuis, R.; van der Krogt, G.; Laptenok, S. P.; Jalink, K.; Wieringa, B.; Fransen, J. A. M. *PLoS One* **2010**, *5*, No. e13862.
(36) Niehörster, T.; Löschberger, A.; Gregor, I.; Krämer, B.; Rahn, H. J.; Patting, M.; Koberling, F.; Enderlein, J.; Sauer, M. *Nat. Methods* **2016**, *13*, 257−262.
(37) Pereiro, I.; Cors, J. F.; Pané, S.; Nelson, B. J.; Kaigala, G. V. *Chem. Soc. Rev.* **2019**, *48*, 1236−1254.
(38) Pereiro, I.; Fomitcheva-Khartchenko, A.; Kaigala, G. V. *Anal. Chem.* **2020**, *92*, 10187−10195.
(39) Sun, Y. S.; Landry, J. P.; Fei, Y. Y.; Zhu, X. D.; Luo, J. T.; Wang, X. B.; Lam, K. S. *Langmuir* **2008**, *24*, 13399−13405.
(40) Olivier, M.; Hollstein, M.; Hainaut, P. TP53 Mutations in Human Cancers: Origins, Consequences, and Clinical Use. *Cold*

Spring Harbor Perspectives in Biology; Cold Spring Harbor Laboratory Press, January 1, 2010; p a001008.
(41) Paik, S.; Kim, C.; Wolmark, N. *N. Engl. J. Med.* **2008**, *358*, 1409−1411.
(42) Ahmed, A. A.; Etemadmoghadam, D.; Temple, J.; Lynch, A. G.; Riad, M.; Sharma, R.; Stewart, C.; Fereday, S.; Caldas, C.; deFazio, A.; Bowtell, D.; Brenton, J. D. *J. Pathol.* **2010**, *221*, 49−56.
(43) Berezin, M. Y.; Achilefu, S. *Chem. Rev.* **2010**, *110*, 2641−2684.
(44) Faratian, D.; Christiansen, J.; Gustavson, M.; Jones, C.; Scott, C.; Um, I.; Harrison, D. J. *J. Visualized Exp.* **2011**, No. 56, No. e3334.
(45) Strickler, S. J.; Berg, R. A. *J. Chem. Phys.* **1962**, *37*, 814−822.
(46) Mechanisms and Dynamics of Fluorescence Quenching. In *Principles of Fluorescence Spectroscopy*; Lakowicz, J. R., Ed.; Springer US: Boston, MA, 2006; Vol. *390*, pp 331−351.
(47) Schuck, P.; Zhao, H. *Methods Mol. Biol.* **2010**, *627*, 15−54.
(48) Arar, N. M.; Pati, P.; Kashyap, A.; Khartchenko, A.; Goksel, O.; Kaigala, G. V.; Gabrani, M. *IEEE Trans. Biomed. Eng.* **2019**, *66*, 2952.
(49) Vauquelin, G. *Br. J. Pharmacol.* **2016**, *173*, 2319−2334.
(50) Dimitrow, E.; Riemann, I.; Ehlers, A.; Koehler, M. J.; Norgauer, J.; Elsner, P.; König, K.; Kaatz, M. *Exp. Dermatol.* **2009**, *18*, 509−515.

https://doi.org/10.1021/acs.analchem.2c01076
Anal. Chem. 2022, 94, 10967−10975